New Journal of Physics
The open-access journal for physics

Gas–liquid two-phase flow patterns in rectangular polymeric microchannels: effect of surface wetting properties

D Huh[1,4], C-H Kuo[3], J B Grotberg[1] and S Takayama[1,2,5]

[1] Department of Biomedical Engineering, University of Michigan, 2200 Bonisteel Blvd, Ann Arbor, MI 48109-2099, USA
[2] Macromolecular Science and Engineering Program, University of Michigan, 2300 Hayward St, MI 48109, USA
[3] Department of Mechanical Engineering, University of Michigan, 2350 Hayward St, Ann Arbor, MI 48109-2125, USA
E-mail: takayama@umich.edu

New Journal of Physics **11** (2009) 075034 (14pp)
Received 13 March 2009
Published 31 July 2009
Online at http://www.njp.org/
doi:10.1088/1367-2630/11/7/075034

Abstract. Here we map gas–liquid two-phase flow regimes observed in polymeric microchannels with different wetting properties. We utilized video and confocal microscopy to examine two-phase flow patterns produced by parallel injection of air and water through a Y-shaped junction into a rectangular microchannel made of poly(dimethylsiloxane) (PDMS). We observed seven flow regimes in microchannels with hydrophobic walls, whereas only two flow patterns were identified in hydrophilic microchannels. Our study demonstrates that surface wettability has a profound influence on the spatial distribution of air and water moving in microchannels.

[4] Current address: Departments of Pathology and Surgery, Harvard Medical School, Karp Family Research Laboratories, #11.005C, 300 Longwood Avenue, Boston, MA 02115, USA.
[5] Author to whom any correspondence should be addressed.

Contents

1. Introduction

Two-phase flows are encountered in a wide range of applications including heat exchangers, oil/gas processing and transport, nuclear and chemical reactors, cryogenics, air pollution control, food production and rocketry. In microfabricated systems, two-phase flows offer new opportunities to enhance and extend the performance of single-phase microfluidics by greatly increasing the rate of heat/mass transfer and preventing sample dispersion. Over the past decade, the potential of two-phase flows at the microscale has gained increasing attention and provided an impetus for the development of multiphase microfluidic systems for a variety of applications such as emulsification [1, 2], electronic chip cooling [3], chemical reactions [4]–[6], flow cytometry [7, 8], material synthesis and fabrication [9]–[14], computation [15, 16], chemical detection/screening [17]–[19] and cell encapsulation/analysis [20]–[23]. This in turn has created the demand for a better understanding of the flow behavior of immiscible fluids inside microchannels, which is crucial for successful design and operation of functional multiphase microfluidic systems.

One of the most conventional ways to characterize two-phase flows is to examine flow regimes defined by distinct spatial distribution of moving fluids. Generally, two-phase flow regimes observed in any given channel depend on several factors including fluid flow rates, fluid properties, channel geometry, channel orientation, surface properties and channel size. For example, early work by Taitel and Dukler [24] related these factors to a model predicting the flow regime transitions and developed a generalized two-phase flow regime map for horizontal gas–liquid two-phase flow. They proposed various criteria for growth, propagation and dissipation of surface waves originated from Kelvin–Helmholtz-type instability as the basis for transitions from stable stratified flow to wavy stratified flow, intermittent flow (slug and plug) and annular dispersed flow. Their subsequent work on gas–liquid two-phase flows in vertical tubes also identified gas–liquid surface tension as one of the factors affecting transitions between different flow patterns [25].

In microscale two-phase flow, dimensional scaling dictates the dominant role of the surface interactions due to the increasing surface-to-volume ratio. Within a confined microchannel, these surface interactions include not only the interfacial interaction between the two phases, but also the interaction of each fluid with the channel walls. As a result, the effect of the surface properties of the microchannel walls becomes prominent, which profoundly influences both the

nature of two-phase flows in microchannels and flow regime transitions. Two parameters that are often used to describe multiphase flow are the confinement number (*Co*) and the Eotvos number (*Eo*).

$$Co = \frac{1}{D}\sqrt{\frac{\sigma}{g(\rho_{\mathrm{L}} - \rho_{\mathrm{G}})}},$$

$$Eo = \frac{(2\pi)^2\sigma}{(\rho_{\mathrm{L}} - \rho_{\mathrm{G}})D^2 g},$$

where D is the hydraulic diameter of the flow channel, σ the surface tension, g the gravitational acceleration and ρ the density of the fluid. These dimensionless numbers represent the ratio of surface tension forces to buoyancy forces, and are often used to characterize the shape of interfaces between different fluids. They have also been employed to describe the transition from macroscale to microscale multiphase flow. For example, Suo and Griffith [26] defined microchannel flow as

$$Co \geqslant 3.3.$$

Brauner and Moalem-Maron [27] used the Eotvos number to define microchannel flow:

$$Eo > 1.$$

Commonplace in these definitions is that the effect of surface tension forces becomes predominant over the buoyancy forces as the size of a channel decreases. Despite the increased effect of surface forces, the focus of previous studies on microscale multiphase flows was primarily on the effect of fluid properties [28], channel geometry [29, 30], orientation [31, 32] and size [31, 33, 34] on the morphology of gas–liquid two-phase flows in small capillary tubes or microchannels fabricated in glass or silicon. Much remains to be learned about how the properties of microchannel surfaces affect the morphology of two-phase flows. Early studies by Damianides and Westwater [35], Graska [36], and Barajas and Panton [37] highlighted that the surface contact angle and surface tension between fluids are important variables in understanding gas–liquid two-phase flow patterns and transitions between different flow regimes in millimeter-sized capillary tubes. There have also been recent reports demonstrating the significant effect of surface properties such as wettability and cleanness on two-phase flow regimes [38] and flow boiling [39] in glass microchannels.

In this paper, we investigate the influence of surface wetting properties on air–water two-phase flows in rectangular microchannels fabricated in one of the most widely used polymeric materials in microfluidics called poly(dimethylsiloxane) (PDMS). Specifically, we varied the hydrophobicity of the PDMS microchannels using a plasma-mediated surface modification method and injected air and water in parallel without premixing to generate high-speed air–water two-phase flows in a horizontal rectangular microchannel that is 300 μm in width, 100 μm in height and 1 cm in length. In this system, confinement number (*Co*) and Eotvos number (*Eo*) were estimated to be 18.2 and 13 109.3, respectively. These numbers clearly indicate that the two-phase flow observed in our microfluidic system is well within the realm of microscale two-phase flow where surface tension forces play a predominant role in understanding flow regimes.

Various flow patterns observed using video microscopy were categorized into flow regime maps under different wetting conditions. We also used confocal microscopy to visualize and better understand the vertical distribution of a liquid phase inside microchannels. We show a dramatic difference in two-phase flow patterns caused by channel hydrophobicity; we found seven flow regimes in hydrophobic microchannels and two in hydrophilic channels.

2. Experimental

2.1. Materials and reagents

PDMS was obtained from Dow Corning Corp. (Midland, MI) and SU8 negative photoresist from MicroChem. Corp. (Newton, MA). Fluorescein sodium salt was purchased from Sigma-Aldrich (St Louis, MO).

2.2. Microchannel fabrication and preparation

Hydrophobic microchannels with a height of 100 μm were created by casting PDMS prepolymer against a photolithographically prepared SU8 mold [7] and then bringing the negative relief patterns in conformal contact with a flat slab of PDMS. To make hydrophilic channels, the recessed microchannel features prepared by casting PDMS against a SU8 master were first bonded to a flat PDMS substrate irreversibly using plasma oxidation [7] to form enclosed microchannels. Immediately before use, the entire device was then treated with oxygen plasma to render the interior surfaces of the microchannel hydrophilic. The degree of channel hydrophilicity was varied by changing the time elapsed from plasma oxidation to the beginning of experiments. Using this method, three rectangular microchannels having different wetting properties were prepared: (i) untreated hydrophobic PDMS surface with a contact angle of 111°, (ii) hydrophilic surface (3 h after plasma oxidation, contact angle ∼35°) and (iii) moderately hydrophilic surface (49 h after oxidation, contact angle ∼77°).

2.3. Flow setup

Air–water two-phase flows were generated by parallel injection of compressed air and deionized (DI) water without premixing as depicted in figure 1. The flow rate of water was controlled by a syringe pump, and air flows were regulated by a flow-meter connected to a compressed air tank. Injected fluid streams and resulting flow patterns were observed in the downstream region using a high-speed camera mounted on an inverted epi-fluorescence microscope. For confocal microscopy, aqueous fluorescein solution with a concentration of 0.001% w/v (in DI water) was used as a working liquid to capture cross-sectional images of two-phase flow patterns.

3. Results and discussion

In a hydrophobic microchannel with a surface contact angle of 111°, we identified seven flow regimes depending on the flow rates of air and water. Typical images of flow patterns captured during the experiments are shown in figure 2. In general, air–water two-phase streams maintain their original stratified flow configuration with various interfacial shapes and different degrees of interfacial stability at moderate water flow rates until the water column in the middle spreads

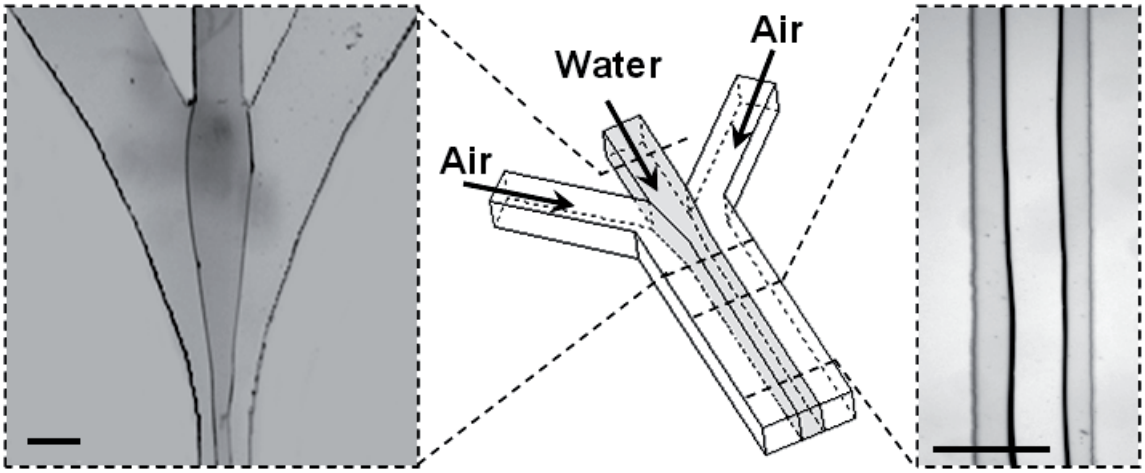

Figure 1. Schematic diagram of an experimental setup used to generate and observe air–water two-phase flow patterns. Water flow was driven by a syringe pump connected to the middle inlet, and gas flows were generated by compressed air injected into the side inlets. The resulting two-phase flow is observed in the downstream region. The micrographs show an example of two-phase flow in a hydrophobic PDMS microchannel. Scale bars, 300 μm.

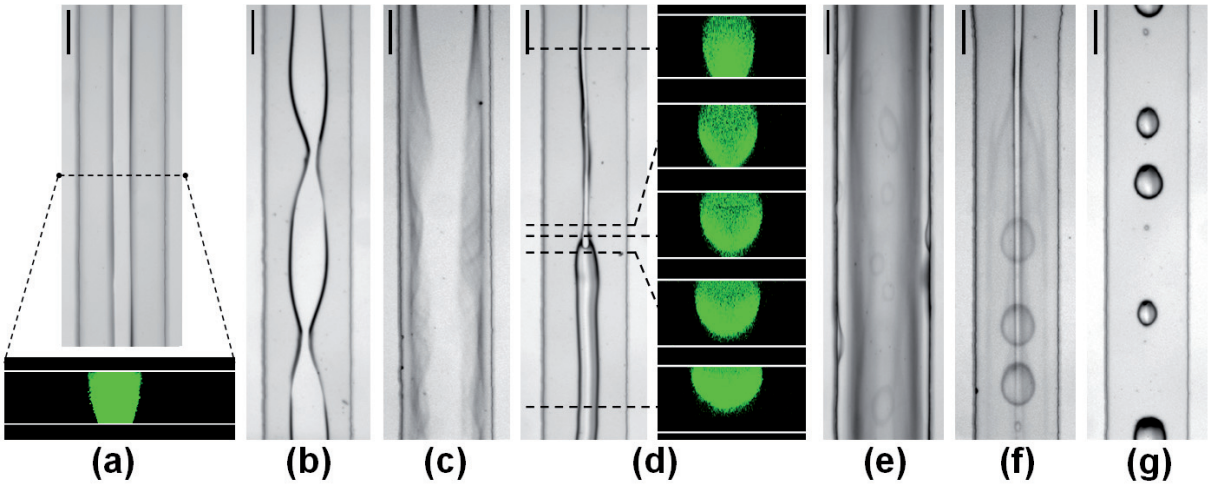

Figure 2. Air–water two-phase flow patterns found in a hydrophobic PDMS channel with a contact angle of 111°. Seven flow regimes were observed with changing fluid flow rates: (a) stable stratified flow, (b) wavy stratified flow, (c) wiggly stratified flow, (d) detached stratified flow, (e) annular-droplet flow, (f) spreading stratified-droplet flow, and (g) break-up. Cross-sectional images shown in (a) and (d) were taken by confocal microscopy. Scale bars, 150 μm.

to the sidewalls at very high flow rates of water or breaks up into small droplets due to two-phase instability as the water flow rate becomes very low. It was noted that there existed maximum flow rates of air and water beyond which the conformal seal between PDMS surfaces failed due to extremely high pressure generated by fluid pumps, and the microchannel became no

longer operational. The seven flow regimes observed in hydrophobic PDMS microchannels include:

1. *Stable stratified flow.* This flow regime is prevalent in hydrophobic microchannels and appears mainly at moderate air and water flow rates. Injected water is focused by air flows to form stable stratification of a water column and two air streams (figure 2(a)). The width of the water column remains the same along the length of the microchannel and changes with the flow rate of water when the air flow rate is maintained constant (or vice versa). The most narrow water column was observed to be as thin as 6 μm. As shown in the cross-sectional images in figure 2(a), the water column is in contact with top and bottom channel walls, and the air–water interface has a convex shape.
2. *Wavy stratified flow.* Wavy stratified flow is characterized by a symmetric varicose wave along the air–water interface, which creates alternating locations of water column expansion and contraction (figure 2(b) and movie 1, available from stacks.iop.org/NJP/11/075034/mmedia). The wavy water column is stably maintained along the center of the microchannel and does not change its shape nor break up into droplets over time at constant air and water flow rates. We observed that the wavelength of the waves found in typical wavy stratified flow was smaller than approximately 600 μm. As fluid superficial velocities were varied, the wavelength ranged between approximately 200 and 600 μm, yet the flow was stable without any temporal changes in the interfacial shape.
3. *Wiggly stratified flow.* This flow pattern occurs at exceedingly high water flow rates and very low airflow rates. In this flow regime, the width of a water stream becomes thicker as a result of increased water flow rate, while the air flow rate is kept constant, and the interface between air and water exhibits wavy patterns undergoing unstable and highly irregular motion as the flow approaches the downstream region of the microchannel (figure 2(c) and movie 2, available from stacks.iop.org/NJP/11/075034/mmedia).
4. *Detached stratified flow.* Interestingly, when the air flow rate is increased while maintaining the liquid flow rate at low levels, the water stream contacts both the top and bottom channel surfaces in the upstream region, but detaches from the bottom floor in the downstream area and forms a convex air–water interface surrounded by ambient air flow as illustrated in the confocal images of figure 2(d) and movie 3, available from stacks.iop.org/NJP/11/075034/mmedia. Both the surface-bound (upstream) and -detached (downstream) columns are stably maintained along the axial line of symmetry without significant changes in their width.
5. *Annular-droplet flow.* Annular-droplet flow consists of a liquid films deposited along the channel sidewalls and air flow through the center (figure 2(e) and movie 4, available from stacks.iop.org/NJP/11/075034/mmedia). The thin liquid films appear to oscillate in a lateral direction, and water droplets that are typically smaller than 50 μm in diameter are entrained in the air stream and travel downstream at high speeds along the core region. This flow configuration becomes more pronounced when the flow rate of water is relatively high and the flow rate of air becomes sufficiently large.
6. *Spreading stratified-droplet flow.* This flow regime is distinguished by co-occurrence of water column and droplets as shown in figure 2(f) and movie 5, available from stacks.iop.org/NJP/11/075034/mmedia. The water column appears to alternate between spreading and break-up at very high frequencies, resulting in the wetting of channel surface

and formation of water droplets along the center of the microchannel. This unique pattern is believed to indicate the onset of two-phase instability as the water flow rate becomes smaller at moderate air flow rates and the water column can no longer maintain its structural integrity.

7. *Break-up*. In this regime, the water column is formed and immediately breaks up into small droplets (figure 2(g) and movie 6, available from stacks.iop.org/NJP/11/075034/mmedia). This takes place for the entire range of the tested air flow rate when the flow rate of water is sufficiently low.

The hydrophobic flow map in figure 4 shows some similarities to the hydrophobic tube results reported in the literature [35, 37], which were generated by using an air–water two-phase flow apparatus comprised of horizontal tubes with an inner diameter of between 1 and 5 mm having several surface hydrophobic and hydrophilic properties. Parallels can be drawn both in overall flow mapping topology and the flow phenomena within each regime between the results reported in these earlier studies and the observations made in our two-phase microfluidic system. For example, the characteristics of rivulet and bubbly flows reported in the work of Barajas and Panton [37] and Taitel and Dukler [24] are almost identical to those of stable stratified and annular-droplet flows observed in our experiments. The ranges of superficial gas and liquid velocities in which these flow patterns are predominant are also similar in the flow map. These similarities are believed to suggest that there exists fundamental mechanics applicable to both macroscale two-phase flow in horizontal pipes and microscale two-phase flow in our microchannels. However, it should be pointed out that the effect of surface forces, which was not factored in the earlier physical modeling of macroscale channel flows, becomes essential in two-phase flow in microchannels. Although beyond the scope of this paper, it is believed that the fundamental modeling scheme introduced by Taitel and Dukler [24] might be extended by incorporating surface force parameters to develop a physical model for the microchannel two-phase flow described in our work.

It is noted that there existed occasional two-phase instabilities accompanying erratic fluid motion when fluids were initially injected into the channel or when fluid flow rates were varied to induce transition from one flow pattern to another. However, the unstable flow behavior subdued rapidly within 10 s, after which two-phase flow remained steady (in the case of stable stratified, wavy stratified and detached stratified flows) or showed particular and predictable patterns with repetitive temporal variations (as in wiggly stratified flow, annular-droplet flow, spreading stratified-droplet flow and break-up). Experimental observations were made after the flow reached this point and no longer exhibited transitional behavior. We did not notice significant variability between experiments, and the same flow regimes were observed reproducibly at their corresponding superficial velocities. However, experiment-to-experiment variability increased near the boundaries between flow patterns, in which case (i) two-phase flow often alternated between two flow patterns neighboring in the flow regime map or (ii) the initially observed flow regime persisted for a few seconds and gave way to its neighboring flow regime.

We did not observe a type of microscale two-phase flow called segmented flow that is often used for mixing and reaction applications in microfluidic systems [53, 54]. This may be attributed to sufficiently higher superficial fluid velocities tested in our work than those used to generate gas–liquid segmented flow reported in the literature. Also, we suspect that our Y-shaped junction at the fluid inlet and the continuous supply of fluids prevented the segmentation of fluids.

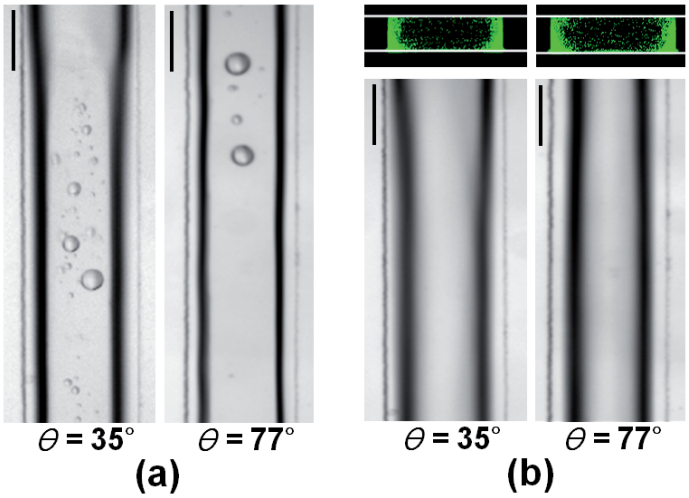

Figure 3. Representative images of two flow regimes identified in hydrophilic channels with different surface wettabilities (contact angle (θ) = 35° and 77°). (a) Annular-droplet flow. (b) Annular flow. Upper insets in (b) show the cross-sectional view of annular flow captured by confocal microscopy. Scale bars, 150 μm.

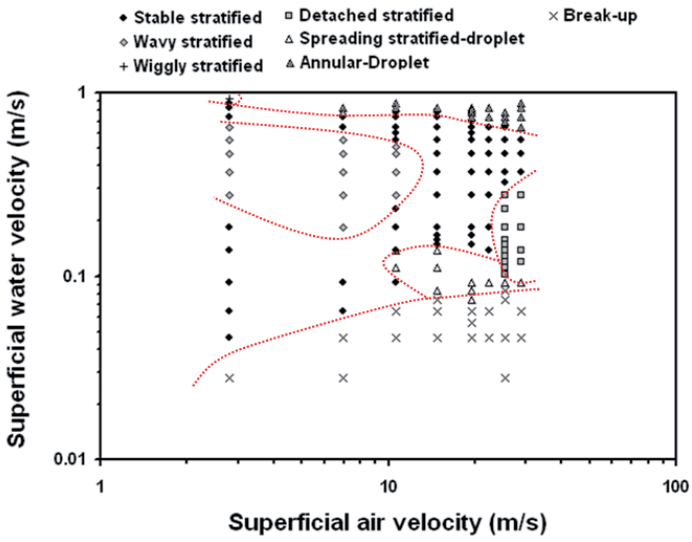

Figure 4. Flow regime map for the hydrophobic microchannel (contact angle = 111°). Dotted lines in the plot indicate transition boundaries.

In contrast to various flow patterns found in hydrophobic channels, only two flow regimes were observed in hydrophilic microchannels, regardless of the contact angle (35° and 75°). In both cases, injected water was quickly redistributed to sidewalls and formed a liquid lining of uniform thickness along the length of the channel as shown by the confocal images in figure 3(b) (upper insets).

1. *Annular-droplet flow.* Annular-droplet flow in hydrophilic channels is slightly different from that in hydrophobic channels in that the water film along the sidewalls

appears to be smoother and the phase boundary between water and air can be seen more clearly as illustrated in figure 3(a), movies 7 and 8, available from stacks.iop.org/NJP/11/075034/mmedia.

2. *Annular flow.* Annular flow is characterized by smooth liquid films on the sidewalls and can be distinguished from annular-droplet flow by the absence of dispersed water droplets in the center region (figure 3(b), movies 9 and 10, available from stacks.iop.org/NJP/11/075034/mmedia).

For a given air flow rate, increasing the flow rate of water shifts the flow regime toward annular flow. The absence of the stratified flow pattern could be related to the experimental observations reported by Triplett *et al* [30] and Chen *et al* [33] that it becomes impossible to form stratified two-phase flow in case of high Eotvos number flow (> 100), as would occur in microchannels under high surface tension conditions.

The degree of hydrophilicity does not affect the type of two-phase flows that can be identified over the range of air and water superficial velocities tested in the experiments. This observation is consistent with previously reported two-phase flow mapping data available in the literature [37]. However, the difference in channel hydrophilicity results in a notable change in the transition boundary between annular-droplet and annular flows. That is, when the contact angle is higher, annular-droplet flow becomes more prominent at low water superficial velocities, indicating more favorable formation of droplets on the channel surfaces presumably due to increased hydrophobicity. As compared with two-phase flows in a hydrophobic microchannel, the duration of transient instabilities observed before fully developed flow regimes formed was much shorter (less than 2 s) in hydrophilic channels, regardless of their surface contact angle. Experimental variability still persisted near the transition boundaries, causing the flow to show characteristics of both annular-droplet and annular flows.

It is known that the PDMS surface rendered hydrophilic by plasma treatment is unstable and gradually recovers its hydrophobicity when exposed to air as a result of diffusion of low molecular weight chains from the bulk PDMS to the surface and their accumulation at the thermodynamically unstable surface [52]. To monitor hydrophobic recovery of hydrophilic PDMS, we measured static contact angle of water on a plasma-treated PDMS surface at different time points after exposure to oxygen plasma (data not shown). We found that surface contact angle gradually increased as a function of time elapsed from plasma treatment. Therefore, careful attention was paid to the timing of experiments; for observation of flow patterns in a microchannel with a surface contact angle of 35° and 75°, we used PDMS microchannels that had been stored in dry air for 3.7 and 47 h, respectively. The duration of conducted experiments was strictly limited to no longer than 1 h to minimize the recovery of hydrophobicity; contact angle changes during the experiments were measured to be smaller than 2°.

The transition between annular flow and annular droplet flow is believed to be dependent on the onset of droplet entrainment from a moving air stream over a liquid film. It was proposed that the primary mechanism of this event may be the shearing off of the crest of Kelvin–Helmholtz-type disturbance wave from low viscosity liquid such as water [40]. In annular air–water flow, this entrainment phenomenon results in water phase traveling along the wall as a liquid film and flowing through the air core as droplets; this is often described by a parameter called entrainment fraction, which represents the combined effects of droplet entrainment and redeposition [41]. Physically, entrainment fraction approaching zero represents pure annular flow without the droplets in the air core. Many researchers have attempted to correlate the entrainment fraction

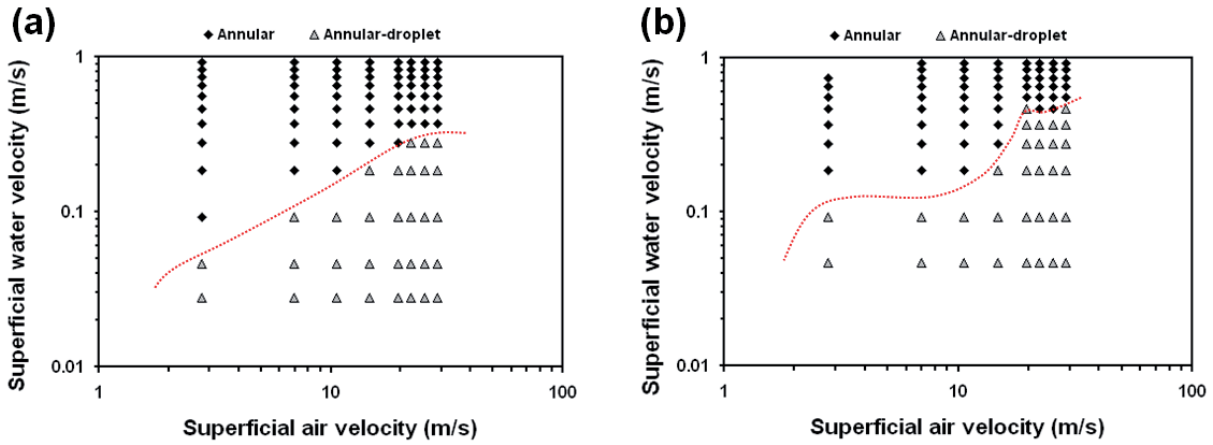

Figure 5. Flow regime maps for the hydrophilic microchannels. (a) Contact angle = 35°. (b) Contact angle = 77°. Dotted lines in the plot indicate transition boundaries.

with the two-phase flow parameters empirically [42]–[44], and found that the correlation is strongly associated with the following two parameters: air-phase Weber number (*We*) and its modified forms comparing air flow velocity-based inertial force to air–water surface tension force, and liquid phase Reynolds number (*Re*). Although the equations for entrainment fraction were developed for macroscale flow conditions in large pipes with diameters on the order of centimeters, they appear to perform adequately in describing the flow transitions in hydrophilic microchannels shown in figures 5(a) and (b). For example, the equation developed by Savant *et al* [44] is given by

$$E = \left(1 - \frac{Re_{\mathrm{ff-lim}}}{Re_{\mathrm{f}}}\right) \tanh\left(a \bullet We^{1.25}\right),$$

$$a = 2.31 \times 10^{-4} Re_{\mathrm{f}}^{-0.35},$$

where E is the entrainment fraction, Re_{f} is the liquid-phase Reynolds number, and limiting liquid film Reynolds number $Re_{\mathrm{ff-lim}}$ is obtained from the following empirical equation.

$$Re_{\mathrm{ff-lim}} = 250 \ln\left(Re_{\mathrm{f}}\right) - 1265.$$

For the range of liquid-phase Reynolds number and air-phase Weber number tested in the current work, the transition boundary line between pure annular flow (i.e. zero entrainment fraction) and annular-droplet flow predicted by these correlation equations is shown in figure 6, along with the boundary line established by actual experimental data shown in figure 5(a). Although there are discrepancies between the predicted and experimentally observed transition lines, they both show a general trend of positive slopes, which extend along increasing superficial air and water velocities. This similarity strongly suggests that the mechanism dictating the transition between pure annular and annular-droplet flows is based on droplet entrainment. We suspect that the mismatch between the estimations and actual experimental data may arise from the fact that the correlation equations were originally developed for macroscale flows in larger circular pipes.

Furthermore, the entrainment fraction correlations may also help explain the shift of flow regime transition line between two different levels of hydrophilicity since it is known that the

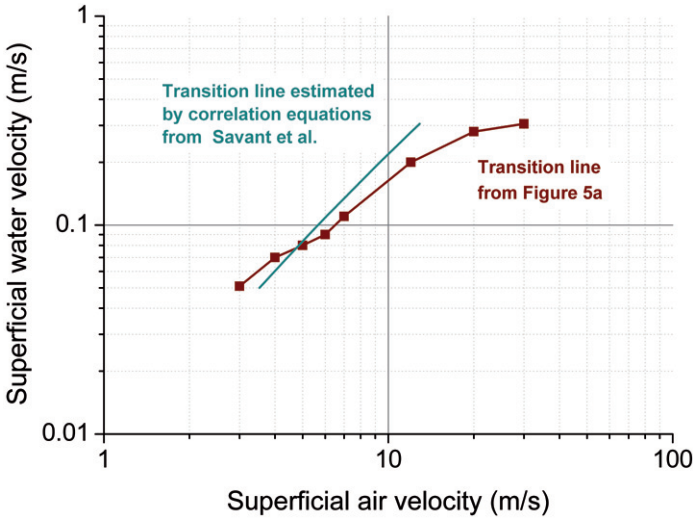

Figure 6. Comparison of flow regime transition boundary between pure annular and annular-droplet flow in the hydrophilic microchannel. The transition line estimated by the correlation equations from Savant *et al* [44] shows a similar trend characterized by a positive slope extending along the increasing superficial air and water velocities, in comparison to the transition line obtained from the experimental observations depicted in figure 5.

surface contact angle affects the water film thickness on the surface of the channel wall [45, 46]; at the same superficial water velocity, differences in surface wettability result in different local water velocity to ensure flow continuity. According to the correlation equation by Savant *et al* [44], this change in local water-phase Reynolds number would shift the transition line between annular flow and annular-droplet flow.

In this work, we have constructed two-phase flow regime maps for the hydrophobic (figure 4) and hydrophilic (figure 5) microchannels. Various flow patterns identified in hydrophobic channels are replaced by two flow regimes in hydrophilic channels, making it evident that the modification of interfacial properties between fluids and channel surfaces has a profound influence on the spatial distribution of fluids moving through a microchannel. Considering that most of the multiple flow regimes found in hydrophobic channels are variations of stratified flow having a water stream confined along the centerline of a channel, we speculate that the drastic difference in flow patterns may be attributed to the inability of hydrophilic microchannels to support the formation of a water column focused by air flows: hydrophilicity causes injected water to wet channel surfaces and spread to corners to minimize interfacial surface area exposed to ambient air [7, 8]. In summary, two factors are believed to promote the high sensitivity of two-phase flow to wall surface properties demonstrated by our microfluidic device. Firstly, the cross-sectional dimensions are sufficiently small that surface forces become more important and play a crucial role in the interaction between different phases. Secondly, the flow configuration where a water column is sheathed by two air streams is inherently sensitive to the forces that affect the integrity of the water column, which include the surface tension forces between the top and bottom channel walls and water, and the pressure and entrainment forces exerted by the air flow. These two factors were not present in similar two-phase flow experiments

reported in the literature [35, 37]. This may explain why, in other work, the topology of the flow regime maps does not show a dramatic change when wettability of the channel wall was altered from hydrophobic to hydrophilic. Although the dominant effect of surface properties increases the complexity of analyzing two-phase flow regimes, it provides an effective means to dramatically change and manipulate the flow pattern within the microchannel, which may enable the development of novel methods for controlling multiphase flows in microfluidic devices. For example, Huh *et al* [8] utilized electrical modulation of surface wettability to switch air–water two-phase flow regimes dynamically and reversibly in elastomeric microchannels. Other methods for controlling microscale multiphase flows include thermocapillarity [47], chemical coating [48]–[50] and surface topography [51].

4. Conclusion

Our work demonstrates that different wetting properties of a microchannel give rise to dramatic changes in the morphological characteristics of two-phase fluid flows at the microscale. We show that surface hydrophobicity in rectangular elastomeric microchannels results in six types of stratification of air–water two-phase flow with various interfacial shapes, and break-up of the water stream into droplets originating from two-phase instabilities. Hydrophilic microchannels were found to cause the water phase to wet channel surfaces immediately and collect at the corners. This configuration led to the formation of annular flow and annular-droplet flow regimes. The drastic difference in flow patterns caused by changes in surface chemistry is particularly relevant to understanding the mechanism of the microfluidic actuation that enables reversible switching of two-phase flow patterns using electrical modulation of surface wettability [13]. Flow regime maps established in this study also allow us to identify the bounds of operation in such microfluidic systems. Moreover, our data open new possibilities to manipulate and engineer high-speed gas–liquid two-phase flows in elastomeric microchannels, which may enable new designs of multiphase microfluidic systems and novel methods for creating and controlling dynamic two-phase flows for various applications. We envision that this will be greatly facilitated by various techniques that are readily available for patterning and modifying the surface chemistry of PDMS. We believe that the transient nature and important timescales of different types of two-phase flows (e.g. time required to form fully developed flow) examined in our study will provide valuable design considerations for the development of microfluidic actuation methods based on surface chemistry changes. The performance of such microsystems can also be extended to higher levels of functionality through on-chip integration with more sophisticated methods for reversibly modulating surface energy such as electrowetting and thermocapillarity.

It should be noted, however, that the experimental work presented in this paper is largely qualitative and focuses mainly on highlighting various flow patterns resulting from changes in surface properties of a microchannel. Understanding the physics of flow patterns and transitions observed in our system will require further analysis based on more standardized parameters in two-phase flow such as void fraction and frictional pressure drop. This will allow us to characterize the distribution of different phases more accurately and eventually develop empirical correlations that can describe and predict the transition from one flow regime to another or practically important processes such as heat and mass transfers.

Acknowledgments

We thank Alan H Tkaczyk and Jonathan W Song for their assistance in setting up compressed air injection systems and flow meters. We also thank Brian Johnson and Mark Burns for providing access to microfabrication facilities. This research was supported by the NSF (BES-0238625) and NIH (HL084370).

References

[1] Utada A S, Lorenceau E, Link D R, Kaplan P D, Stone H A and Weitz D A 2005 *Science* **308** 537
[2] Sugiura S, Nakajima M, Tong J H, Nabetani H and Seki M 2000 *J. Colloid Interface Sci.* **227** 95
[3] Zhang L, Koo J M, Jiang L, Asheghi M, Goodson K E, Santiago J G and Kenny T W 2002 *J. Microelectromech. Syst.* **11** 2002
[4] Song H, Chen D L and Ismagilov R F 2006 *Angew. Chem., Int. Ed. Engl.* **45** 7336
[5] Gunther A and Jensen K F 2006 *Lab Chip* **6** 1487
[6] Hibara A, Iwayama S, Matsuoka S, Ueno M, Kikutani Y, Tokeshi M and Kitamori T *Anal. Chem.* **77** 943
[7] Huh D, Tung Y-C, Wei H-H, Grotberg J B, Skerlos S J, Kurabayashi K and Takayama S 2002 *Biomed. Microdev.* **4** 141
[8] Huh D, Tkaczyk A H, Bahng J H, Chang Y, Wei H-H, Grotberg J B, Kim C-J, Kurabayashi K and Takayama S 2003 *J. Am. Chem. Soc.* **125** 14678
[9] Yen B K H, Gunther A, Schmidt M A, Jensen K F and Bawendi M G 2005 *Angew. Chem., Int. Ed. Engl.* **44** 5447
[10] Zheng B, Roach L S and Ismagilov R F 2003 *J. Am. Chem. Soc.* **125** 11170
[11] Dendukuri D, Tsoi K, Hatton T A and Doyle P S 2005 *Langmuir* **21** 2113
[12] Li W, Pharn H H, Nie Z, MacDonald B, Guenther A and Kumacheva E 2008 *J. Am. Chem. Soc.* **130** 9935
[13] Millman J R, Bhatt K H, Prevo B G and Velev O D 2005 *Nat. Mater.* **4** 98
[14] Zhao B, Viernes N O L, Moore J S and Beebe D J 2002 *J. Am. Chem. Soc.* **124** 5284
[15] Fuerstman M J, Garstecki P and Whitesides G M 2007 *Science* **315** 828
[16] Prakash M and Gershenfeld 2007 *Science* **315** 832
[17] Lau B T C, Baitz C A, Dong X P and Hansen C L 2007 *J. Am. Chem. Soc.* **129** 454
[18] Chen D, Du W, Liu Y, Liu W, Kuznetsov A, Mendez F E, Philipson L H and Ismagilov R F *Proc. Natl Acad. Sci. USA* **105** 16843
[19] Li L, Mustafi D, Fu Q, Tereshko V, Chen D L, Tice J D and Ismagilov R F *Proc. Natl Acad. Sci. USA* **103** 19243
[20] Clausell-Thormos J *et al* 2008 *Chem. Biol.* **15** 875
[21] Huebner A, Srisa-Art M, Holt D, Abell C, Hollfelder F, deMello A J and Edel J B 2007 *Chem. Commun.* 1218
[22] Boedicker J Q, Li L, Kline T R and Ismagilov R F *Lab Chip* **8** 1265
[23] Huh D, Fujioka H, Tung Y-C, Futai N, Paine R, Grotberg J B and Takayama S 2007 *Proc. Natl Acad. Sci. USA* **104** 18886
[24] Taitel Y and Dukler A 1976 *AIChE J.* **22** 47
[25] Taitel Y, Bornea D and Dukler A 1980 *AIChE J.* **26** 345
[26] Suo M and Griffith P 1964 *J. Basic Eng.* **86** 576
[27] Brauner N and Moalem-Maron D 1992 *Int. Commun. Heat Mass Transfer* **19** 29
[28] Serizawa A, Feng Z and Kawara Z 2002 *Exp. Therm. Fluid Sci.* **26** 703
[29] Chung P M Y, Kawaji M, Kawahara A and Shibata Y 2004 *J. Fluids Eng.—Trans. ASME* **126** 546
[30] Triplett K A, Ghiaasiaan S M, Abdel-Khalik S I and Sadowski D L 1999 *Int. J. Multiph. Flow* **25** 377
[31] Fukano T and Kariyasaki A 1993 *Nucl. Eng. Des.* **141** 59
[32] Liu D and Wang S 2008 *Ind. Eng. Chem. Res.* **47** 243

[33] Chen L, Tian Y S and Karayiannis T G 2005 *J. Process. Mech. Eng.* **219** 167–81
[34] Chung P M Y and Kawaji M 2004 *Int. J. Multiph. Flow* **30** 735
[35] Damianides C A and Westwater J W 1988 *Proc. 2nd UK Natl Conf. on Heat Transfer* vol II pp 1257–68
[36] Graska M L 1986 *MS Thesis* University of Illinois at Urbana-Champaign
[37] Barajas A M and Panton R L 1993 *Int. J. Multiph. Flow* **19** 337
[38] Dreyfus R, Tabeling P and Willaime H 2003 *Phys. Rev. Lett.* **90** 144505
[39] Choi C and Kim M H 2008 *J. Micromech. Microeng.* **18** 105016
[40] Ishii M and Grolmes M A 1975 *AIChE J.* **21** 308
[41] Kataoka I, Ishii M and Mishima K 1983 *J. Fluid Eng.—Trans. ASME* **105** 230
[42] Ishii M and Mishima K 1989 *Int. J. Heat Mass Transfer* **32** 1835
[43] Pan L and Hanratty T J 2002 *Int. J. Multiph. Flow* **28** 363
[44] Savant P, Ishii M and Mori M 2008 *Nucl. Eng. Des.* **238** 1342
[45] Mikielewicz J and Moszynski J R 1976 *Int. J. Heat Mass Transfer* **19** 171
[46] EL-Genk M S and Saber H 2001 *Int. J. Heat Mass Transfer* **44** 2809
[47] Darhuber A A, Valentino J P, Troian S M and Wagner S 2003 *J. Micromech. Syst.* **12** 873
[48] Zhao B, Moore J S and Beebe D J 2001 *Science* **291** 1023
[49] Zhao B, Viernes N O L, Moore J S and Beebe D J 2002 *J. Am. Chem. Soc.* **124** 5284
[50] Abbott N L, Folkers J P and Whitesides G M 1992 *Science* **257** 1380
[51] Lafuma A and Quere D 2003 *Nat. Mater.* **2** 457
[52] Bodas D and Khan-Malek C 2007 *Sensors Actuators* B **123** 368
[53] Kreutzer M T, Gunther A and Jensen K 2008 *Anal. Chem.* **80** 1558
[54] De Mas N, Gunther A, Schmidt M A and Jensen K F 2009 *Ind. Eng. Chem. Res.* **48** 1428